Computational and Experimental Study of Time-Averaged Characteristics of Positive and Negative DC Corona Discharges in Point-Plane Gaps in Atmospheric Air

Nuno G. C. Ferreira, Pedro G. C. Almeida, Mikhail S. Benilov, Victor A. Panarin, Victor S. Skakun, Victor F. Tarasenko, and George V. Naidis

***Abstract*— The use of stationary solvers instead of approximate solution methods or time-dependent solvers, which are standard tools in gas discharge modeling, allows one to develop a very fast and robust numerical model for studying the time-averaged characteristics of dc corona discharges. Such an approach is applied to dc corona discharges in point-plane gaps in ambient air. A wide range of currents of both voltage polarities and various gap lengths are investigated, and the simulation results are validated by comparing the computed current–voltage characteristics and spatial distributions of the radiation intensity with experimental results. Specific features of the numerical and experimental results at both polarities are discussed.**

***Index Terms*— Corona, current-voltage characteristics, dc discharges.**

I. Introduction

TIME-DEPENDENT solvers are standard tools in the modeling of corona discharges, as well as in gas discharge modeling in general. Time-dependent computations give detailed information on spatiotemporal distributions of plasma parameters and are indispensable for studies of pulsed coronas; for example, computational studies of pulsed regimes of dc corona discharges in point-plane air gaps in the framework of non-stationary approaches are reported in recent works [1]–[4]. Time-dependent solvers can also be used for the computation of time-averaged characteristics of dc corona discharges in the framework of stationary corona discharge models; see [5], [6]. However, such solvers are highly, and in many cases, prohibitively, computationally intense. Therefore, stationary characteristics of dc corona discharges are calculated in most cases by means of various approximate methods; see [5], [7]–[12].

An alternative to using time-dependent solvers for stationary corona discharge models is to employ stationary solvers, which solve steady-state equations describing the stationary discharge by means of an iterative process unrelated to time relaxation. Stationary solvers offer important advantages in simulations of steady-state discharges. In particular, they are not subject to the Courant–Friedrichs–Lewy criterion or analogous limitations on the mesh element size, which allows one to dramatically speed up simulations.

In [13], a stationary solver was used for the computation of inception of corona discharges. In this work, the method [13] is modified in a way to be applicable to calculation of time-averaged characteristics of dc positive and negative corona discharges in a wide current range. Special attention is paid to the validation of the new method. Somewhat surprisingly, it seems that experimental data on corona discharges reported in the literature beyond the simplest 1-D wire-cylinder configuration are insufficient for an accurate quantitative comparison, since not all relevant geometrical parameters are indicated. Therefore, special experiments have been performed on point-to-plane coronas in a wide current range of currents of both polarities. The computed current-voltage characteristics and spatial distributions of the radiation intensity for both polarities and various values of the discharge gap have been compared with experimental results. Specific features of the numerical and experimental results at both polarities are discussed.

II. Numerical Method

We consider a conventional system of equations describing low-current discharges in high-pressure air, which comprises equations of conservation and transport of charged species and the Poisson equation

$$\nabla \cdot \mathbf{J}_\alpha = S_\alpha \quad (\alpha = e, \mathrm{O}_2^+, \mathrm{O}_2^-, \mathrm{O}^-, \mathrm{O}_3^-). \tag{1}$$

$$\varepsilon_0 \nabla^2 \phi = -e \sum_\alpha Z_\alpha n_\alpha. \tag{2}$$

$$\mathbf{J}_\alpha = -D_\alpha \nabla n_\alpha - Z_\alpha n_\alpha \mu_\alpha \nabla \phi. \tag{3}$$

Manuscript received July 10, 2020; revised September 10, 2020; accepted October 9, 2020. Date of publication November 3, 2020; date of current version December 11, 2020. This work was supported in part by FCT of Portugal under Project UIDP/50010/2020, in part by the European Regional Development Fund through the Program Madeira 2014–2020 under Project PlasMa-M1420-01-0145-FEDER-000016 (UMa), in part by the State Assignment under Project 13.1.4 (HCEI), and in part by RFBR under Grant 20-02-00320 (JIHT). The review of this article was arranged by Senior Editor F. Taccogna. *(Corresponding author: Mikhail S. Benilov.)*

Nuno G. C. Ferreira, Pedro G. C. Almeida, and Mikhail S. Benilov are with the Departamento de Física, Faculdade de Ciências Exatas e da Engenharia, Universidade da Madeira, 9000 Funchal, Portugal, and also with the Instituto de Plasmas e Fusão Nuclear, Instituto Superior Técnico, Universidade de Lisboa, 1049-001 Lisbon, Portugal (e-mail: benilov@staff.uma.pt).

Victor A. Panarin, Victor S. Skakun, and Victor F. Tarasenko are with the Institute of High Current Electronics SB RAS, 634055 Tomsk, Russia.

George V. Naidis is with the Joint Institute for High Temperatures, Russian Academy of Sciences, 125412 Moscow, Russia.

Color versions of one or more of the figures in this article are available online at https://ieeexplore.ieee.org.

Digital Object Identifier 10.1109/TPS.2020.3031076

Here, subscript α identifies charged species; n_α, $\mathbf{J}_\alpha$, D_α, μ_α, S_α, and Z_α are, respectively, number density, density of transport flux, diffusion coefficient, mobility, net volume rate of production, and charge number of species α; ϕ is the electrostatic potential; e is the elementary charge; and ε_0 is the permittivity of free space. The conservation equations, (1), are written for the steady-state case. Equations of transport of charged species, (3), are written in the local-field approximation, i.e., with the electron transport and kinetic coefficients being assumed to depend on the local reduced electric field E/N only. The source terms S_α in equations for electrons and positive ions include, in addition to terms describing production of these species in collisional processes, the photoionization term S_{ph}. The latter is evaluated by means of the three-exponential Helmholtz model [14] $S_{\mathrm{ph}}(\mathbf{r}) = \sum_{j=1}^{3} S_{\mathrm{ph}}^{(j)}(\mathbf{r})$, with each of the terms satisfying the Helmholtz partial differential equation

$$\nabla^2 S_{\mathrm{ph}}^{(j)}(\mathbf{r}) - \left(\lambda_j p_{\mathrm{O}_2}\right)^2 S_{\mathrm{ph}}^{(j)}(\mathbf{r}) = -A_j p_{\mathrm{O}_2}^2 I(\mathbf{r}) \quad (j = 1, 2, 3). \tag{4}$$

Here, A_j and λ_j are constants (parameters of the three-exponential fit function) given in [14], p_{O_2} is the partial pressure of molecular oxygen, and $I(\mathbf{r})$ is the product of ξ the probability of ionization of a molecule at photon absorption and the local photon production rate.

The kinetic scheme of plasmachemical processes is the same as the one formulated in [13], with a few minor changes. Note that in [13] this scheme was validated by a comparison of the computed inception voltage of corona discharges with several sets of experimental data on positive and negative glow coronas between concentric cylinders in a wide range of pressures and diameters of the cylinders and on positive coronas in the rod-to-plane configuration. The scheme takes into account the electrons, one species of positive ions, which are represented mostly by O_2^+, and three species of negative ions, O_2^-, O^-, and O_3^-, and comprises the following processes: electron impact ionization, two-body (dissociative) attachment, three-body attachment, photoionization, collisional detachment from O_2^-, associative detachment from O^-, charge transfer from O^- to O_2^-, conversion of O^- to O_3^-, and ion-ion and electron-ion recombination. The transport coefficients of the electrons were evaluated in the same way as in [13] (the mobility was taken from [15] and the longitudinal and transversal electron diffusion coefficients were evaluated with the use of the online version of the Bolsig+ solver [16] and the cross sections [17]).

Special care is required as far as the ion transport coefficients are concerned: while values of ion mobilities do not affect appreciably the inception voltage of corona discharges, which was the parameter computed in [13] and found to be in a good agreement with the experiment, values of ion mobilities in the drift zone do affect the corona current–voltage characteristics. Complex ions O_4^+, O_4^-, and cluster ions (comprising one or several $\mathrm{H_2O}$ molecules), with typical mobilities in the range $2.0-2.4\ \mathrm{cm^2\,V^{-1}\,s^{-1}}$ [18], may appear in the drift zone of corona discharges in air. In order to take it into account, the mobilities of the positive ions O_2^+ and the negative ions O_2^- were set equal to $2.2\ \mathrm{cm^2\,V^{-1}\,s^{-1}}$ (which is slightly different from the values of 2.51 and $2.16\ \mathrm{cm^2\,V^{-1}\,s^{-1}}$, given in [18] for the individual mobilities of the ions O_2^+ and O_2^-).

According to [19], the reduced mobility of O^- varies between 3.66 and $5.24\,\mathrm{cm^2\,V^{-1}\,s^{-1}}$ over the reduced field range up to 100 Td (there is no data for higher reduced fields). In principle, such variations can be readily introduced in the numerical model. Since, however, a constant value is used for the mobility of O_2^- (and complex/cluster ions), and given that the above variation is not huge, a constant value of $5.2\ \mathrm{cm^2\,V^{-1}\,s^{-1}}$ is used for the reduced mobility of O^- in order to be consistent. According to [20], the reduced mobility of O_3^- varies between 2.5 and $3.1\ \mathrm{cm^2\,V^{-1}\,s^{-1}}$ over the reduced field range up to 100 Td, and varies between 3.1 and $2.9\,\mathrm{cm^2\,V^{-1}\,s^{-1}}$ over the reduced field range between 100 Td and 240 Td. In this work, the reduced mobility of O_3^- was set equal to $2.7\ \mathrm{cm^2\,V^{-1}\,s^{-1}}$, which is a value characteristic of reduced field of the order of 50 Td, where these ions are expected to be most abundant.

The diffusion coefficients of all ion species are related to the mobilities through Einstein's relation with the corresponding ion temperatures, which were evaluated by means of the Wannier equation. Temperature T of the neutral gas is assumed to be constant; results reported in this work refer to $T = 300$ K.

The boundary conditions are conventional and the same as in [13] except that the number densities of the negative ions at the cathode and of the positive ions at the anode were set equal to zero, instead of being defined by the chaotic flux. (We note right now that the effect of this change on the solution was insignificant, which increases the reliability of the results, given that this boundary condition cannot be formulated in an exact way.)

The numerical implementation is based on the use of stationary solvers and was developed on the computational platform COMSOL Multiphysics. The following interfaces were used: Electrostatics (the Poisson equation), Transport of Diluted Species, or TDS (the equations of conservation and transport of charged species), and Coefficient Form (the Helmholtz equations). The reactions considered within the kinetic scheme were taken into account as production/loss terms in the TDS interface. The default consistent stabilization (streamline and crosswind diffusion) was maintained activated in the TDS interface.

Two formulations of the species conservation equations have been tested: the original formulation, where the dependent variables are the species number densities, and the logarithmic formulation, where the dependent variables are logarithms of the species number densities. (The logarithmic formulation ensures that the number density of any of the species is never negative and is frequently used in the modeling of cold gas discharges, in particular, it was used in the preceding work [13].) The original formulation has been found to be much more efficient for the steady-state modeling, performed in this work, and was used in all the simulations reported here. Note that it was the use of the original formulation that made possible the above-described change in the boundary condition

for the number densities of the negative ions at the cathode and of the positive ions at the anode.

A natural control parameter in the modeling is the corona voltage. However, at low discharge currents the corona voltage remains virtually the same (and very close to the inception voltage) as current varies over orders of magnitude. In this situation, the discharge current is a more suitable control parameter than the voltage. Therefore, the model allowed both corona voltage or current serving as a control parameter, with switching between these two parameters in an easy and seamless way. The latter was achieved with the use of the Weak Form interface of COMSOL Multiphysics.

The solution computed for each value of the corona voltage or current was used as an initial approximation for the computation with the next value. Calculations of the set of solutions describing a wide range of corona voltages/currents for each gap were performed separately for the positive and negative polarities. For each polarity, the first step was to find a solution describing the corona inception, as described in [21]. The second step was a series of computations with the corona current serving as a control parameter and being gradually increased. When the corona voltage has increased by about 200 V with respect to the inception voltage, the control parameter was switched to the corona voltage U and the computation proceeded with U being gradually increased until the whole range of current values of interest has been covered.

III. Experimental Setup

The above-described numerical method requires experimental validation. Somewhat surprisingly, it seems that experimental data on corona discharges reported in the literature beyond the simplest one-dimensional wire-cylinder configuration are insufficient for an accurate quantitative comparison: not all relevant geometrical parameters are indicated. For example, the rod length is a parameter omitted in experimental publications on corona discharges in the rod-to-plane configuration; e.g., works [22], [23] and their discussion in [13]. As another example, one can mention wire coronas: they are very sensitive to the environment (see [24]), meaning that the electrostatic boundary conditions are not well defined.

Therefore, special experiments have been performed on point-to-plane coronas in a wide range of currents of both polarities. The experimental setup was analogous to those typically used for studying corona discharges in point-plane gaps. It consists of needle and flat electrodes, power source, and recording equipment, and is shown in Fig. 1. A dc voltage source 5 is connected to the needle 1 through a resistance of $R = 18$ MΩ. The polarity of the voltage source could be either positive or negative and the source can smoothly change the voltage U from 1 to 25 kV. In series with the plane electrode, the shunt is switched on through a resistance of $R_3 = 1$ kΩ. The voltage across the gap is measured using a high voltage probe formed by the resistances R_1 and R_2. The electrode with a small radius of curvature is made of a 50 mm long copper needle with a diameter of 3 mm, having a tip radius of 0.2 mm (see Fig. 2). The plane electrode is mounted at a distance from the tip of the needle varying from 5 to 14 mm.

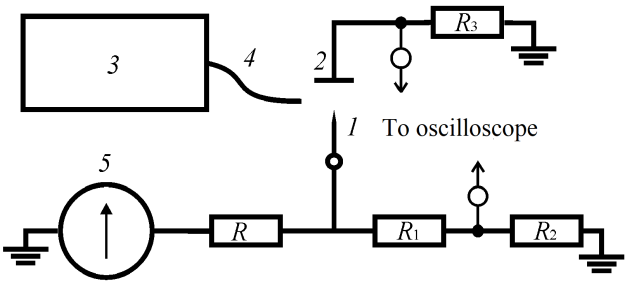

Fig. 1. Experimental design. 1—needle, 2—plane electrode, 3—spectrometer with a light guide 4 or a camera, 5—dc voltage source. R is the resistance limiting the discharge current; R_1 and R_2 are the resistances of the voltage divider; R_3 is the resistance of the current shunt.

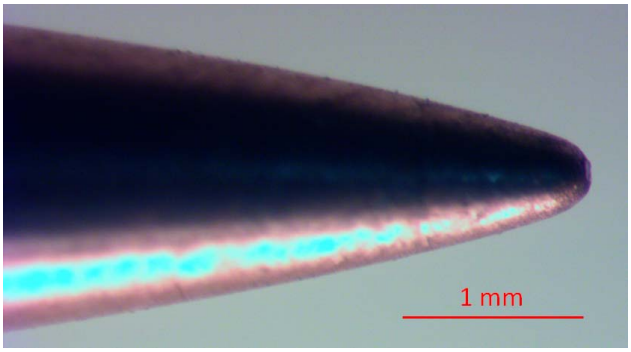

Fig. 2. Needle electrode.

The measured parameters were the corona current, the voltage at the tip, and the radiation intensity distribution. The variation of voltage and current with time was recorded using a TDS 3034 oscilloscope (Tektronics, Inc.), a high-voltage probe, and a shunt. Moreover, when recording the discharge current, its average value was determined using the corresponding recording mode of the TDS 3034 oscilloscope. The average discharge current for each point was determined within 40 μs at a constant voltage across the gap, the value of which was set with an accuracy better than 1%. The voltage change during measurements of the average current also did not exceed 1%. Note that individual short pulses that were generated during 40 μs, in particular Trichel pulses, were taken into account when measuring the average corona discharge current. However, the generation of individual short pulses did not have a noticeable effect on the average corona discharge current.

Photos of the corona discharge were obtained with a Canon PowerShot SX 60 HS digital camera in the single-shot mode with an exposure time of 15 s. Corona emission spectra were recorded using an assembly that included a collimating lens with a focal length of 30 mm, an optical fiber with a known transmission spectrum, and an HR2000 + ES spectrometer (Ocean Optics, Inc.) based on a multichannel CCD line Sony ILX511B (operating range 200–1100 nm, spectral half-width of the hardware function $\sim$ 1.33 nm).

The experiments were conducted in ambient atmospheric air under normal conditions. As the current–voltage

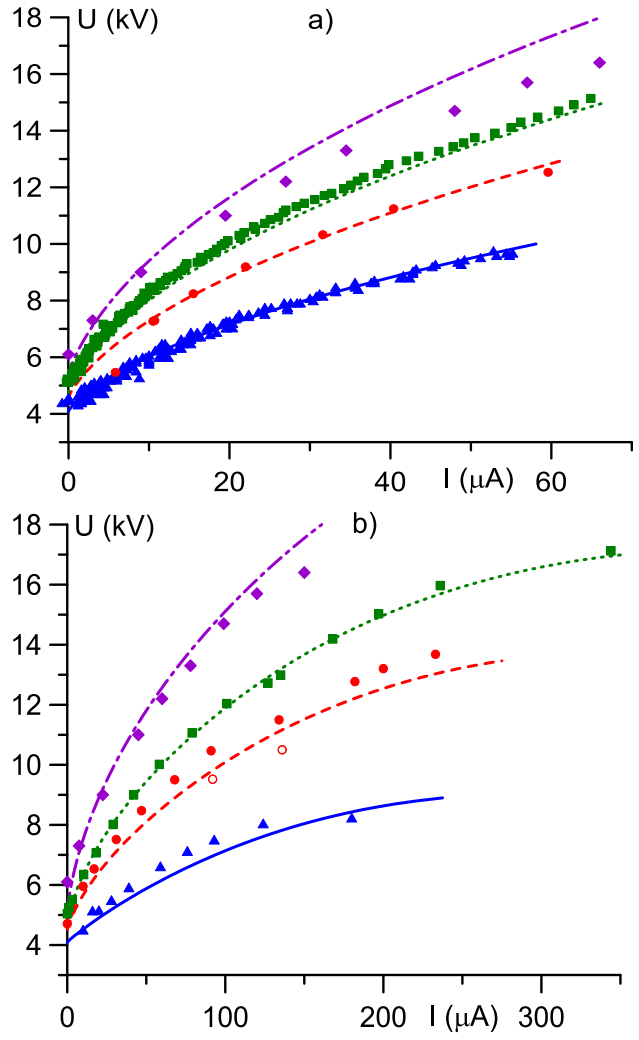

Fig. 3. Current–voltage characteristics of (a) positive and (b) negative corona discharges. Points: experiment. Lines: modeling. Triangles, solid: $d = 5$ mm. Closed and open circles, dashed: 8 mm (see also text). Squares, dotted: 10 mm. Diamonds, dash-dotted: 14 mm.

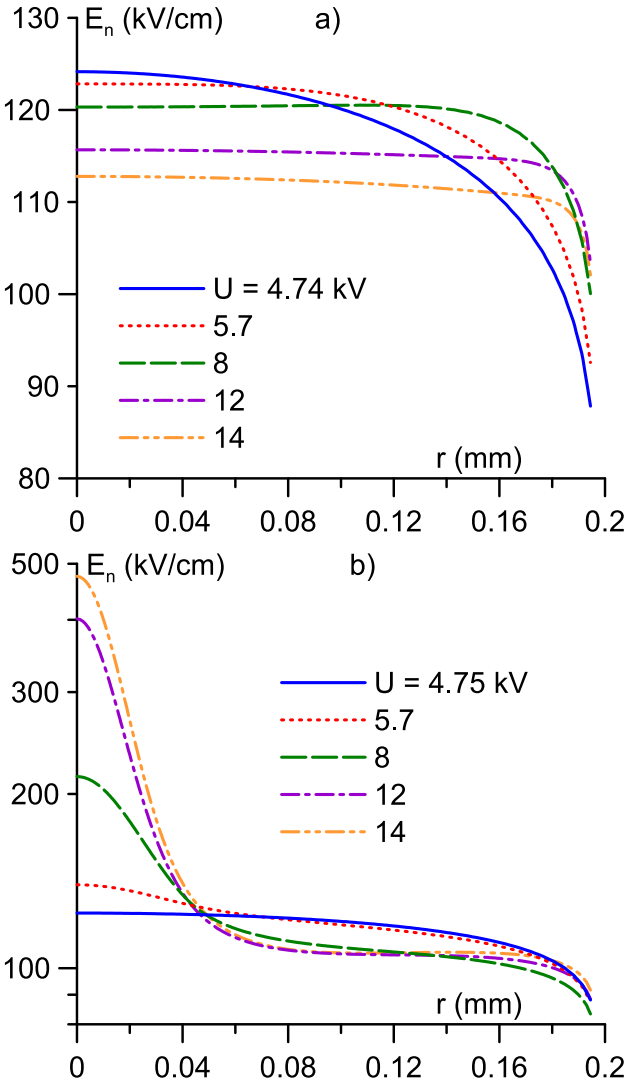

Fig. 4. Distributions of the normal electric field along the needle surface at various applied voltages in (a) positive and (b) negative corona discharges. $d = 10$ mm.

characteristics (CVCs) are influenced by variation of pressure and humidity of ambient air, depending on weather conditions, the CVCs were measured during one day, in a time interval as short as possible.

IV. Results and Discussion

The computed (lines) and measured (points) CVCs of corona discharges both for positive and negative polarities of the tip electrode are shown in Fig. 3 for several values of the gap length d. Experimental points shown by triangles, closed circles, squares, and diamonds were obtained in the same day at the temperature of 21 °C, pressure of 747 mmHg, and air humidity of about 50%. For negative corona in one of the gaps, $d = 8$ mm, also shown are experimental data (open circles) measured in a different day at different atmospheric conditions: the temperature of 20 °C, pressure of 740 mmHg, and humidity of about 60%.

The secondary electron emission coefficient in the modeling was set equal to 10^{-4}; a value which allowed to obtain the ignition corona voltage in agreement with the experiment. Note that the effect of variations of the secondary electron emission coefficient on inception of positive and negative corona between concentric cylinders was investigated in [13] and it was found that the agreement with experiment was lost for values of the secondary electron emission coefficient higher than 10^{-4}.

In all the cases, the calculated values agree well with the measured data. Note that the coefficient of determination R^2 equals 0.989, 0.967, 0.994, and 0.897 for the gaps of 5, 8, 10, and 14 mm, respectively, in the case of positive corona and 0.920, 0.975, 0.999 and 0.967 in the case of negative corona. (Here, the coefficient of determination is defined as $R^2 = 1 - \mathrm{SS_{res}}/\mathrm{SS_{tot}}$, where $\mathrm{SS_{res}}$ is the residual sum of squares and $\mathrm{SS_{tot}}$ is the total sum of squares, so that $R^2 = 1$ corresponds to the exact match between the modeling and the experiment.)

A comparison of CVCs of positive and negative coronas shows that their inception voltages, for the same gap d, are

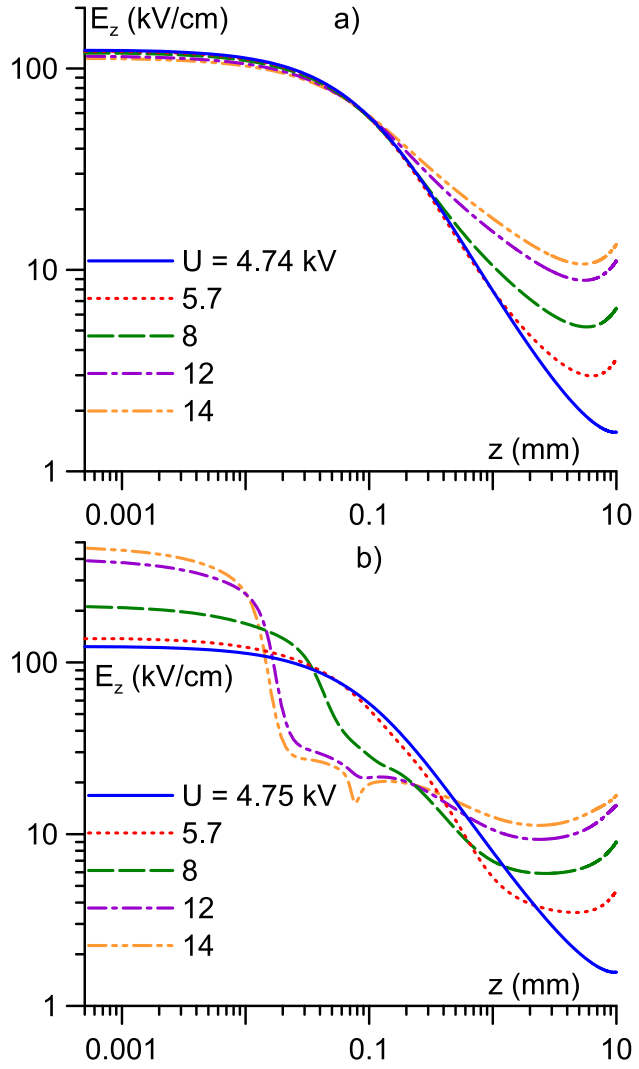

Fig. 5. Distributions of the axial electric field along the discharge axis at various applied voltages in (a) positive and (b) negative corona discharges.

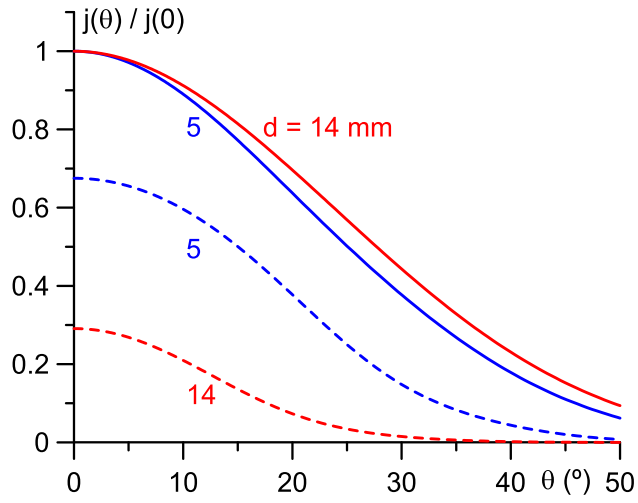

Fig. 6. Distributions of normalized total (solid) and electron (dashed) current densities in negative corona discharges over the plane electrode.

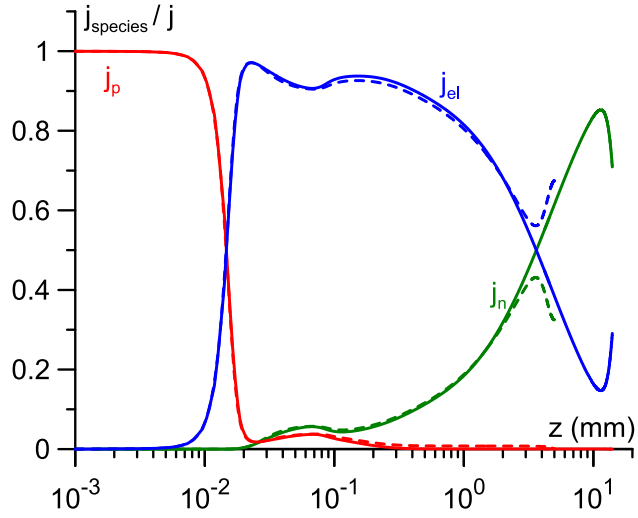

Fig. 7. Distributions of normalized densities of the current transferred by the positive ions, the negative ions, and the electrons in negative corona discharges along the discharge axis. Dashed: $d = 5$ mm. Solid: $d = 14$ mm.

rather close. However, the current I_n in a negative corona is two to three times higher than the current I_p in a positive corona at the same applied voltage U, the ratio I_n/I_p decreasing with increase in d. Note that a similar effect of the gap length variation has been observed in the experiment [25]. Note also that the differences in current for different corona polarities reported in the recent experiment [26] were smaller than in this work, which is consistent with the longer gap being used in [26] (20 mm).

Results of simulation show a substantial difference in spatial distributions of time-averaged electric field inside positive and negative corona discharges. Distributions of the normal electric field E_n along the needle surface for both polarities, $d = 10$ mm, and various applied voltages are shown in Fig. 4. Here, r is the distance to the discharge axis. In the case of positive coronas [Fig. 4(a)], the profiles broaden with increase in U and the electric field E_0 at the tip (at $r = 0$) decreases slightly. An opposite trend takes place in negative coronas, where an increase in U results in a substantial (up to four times in the voltage range considered) increase of E_0 and appearance of a pronounced maximum close to the axis. Note that similar profiles of E have been obtained in simulations [6] of positive and negative dc air coronas in a sphere-plane gap.

Distributions of the axial electric field E_z along the axis are shown for both polarities, various applied voltages, and $d = 10$ mm in Fig. 5. Here z is the distance from the tip of the needle electrode. In the case of positive corona [Fig. 5(a)], the electric field in the ionization region (the region where E exceeds the critical field, of about 25 kV cm^{-1}, which corresponds to equality of ionization and attachment coefficients) depends on U rather weakly, while the electric field in the drift region increases with increasing U. Such a pattern is similar to that in corona discharges in axially symmetric wire-cylinder gaps [27]. Note that the computed electric field in the ionization region being virtually independent of the applied voltage is consistent with the classic Kaptzov assumption. This assumption, which states that the steady state

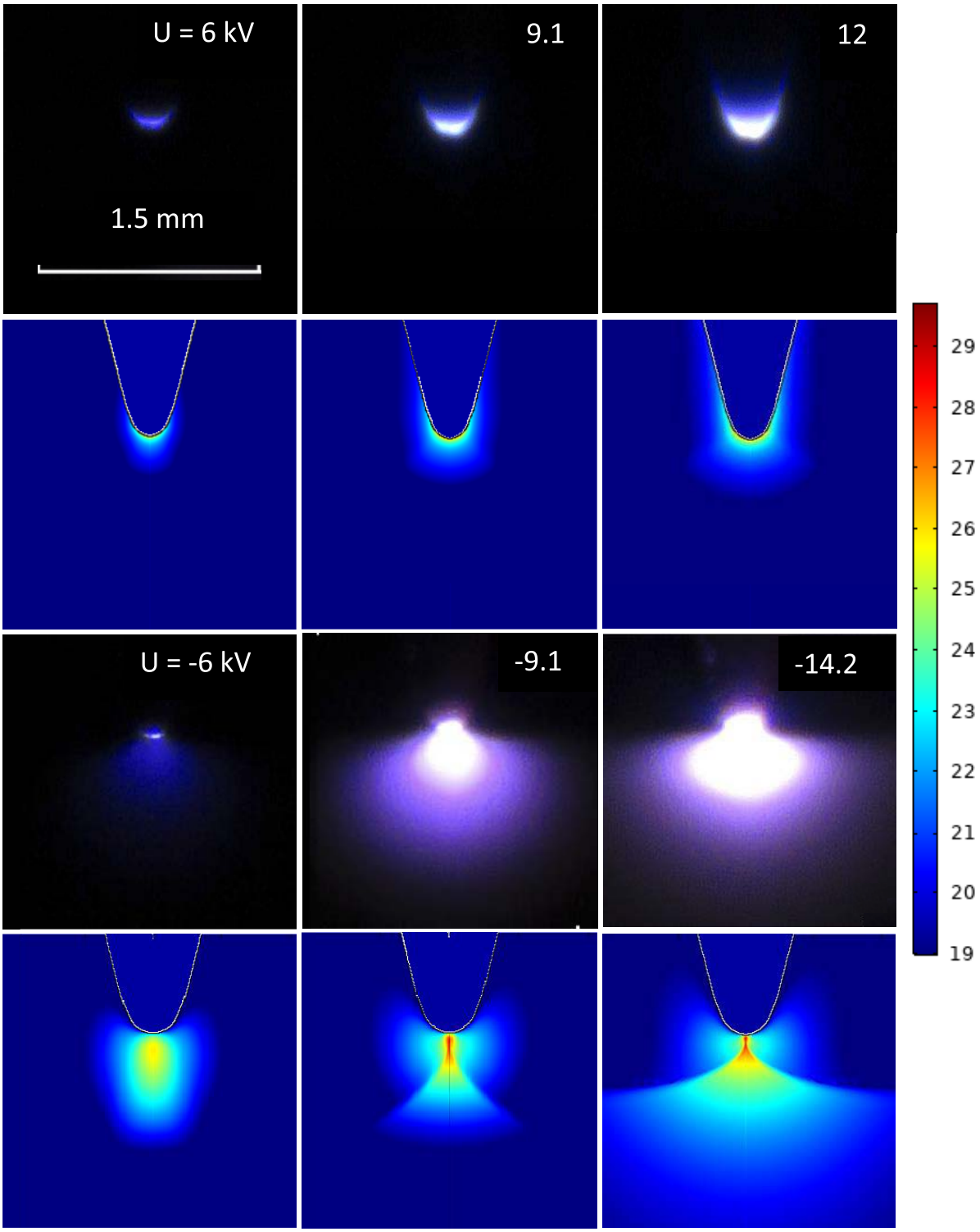

Fig. 8. Images of corona discharges and computed distributions of the rate of excitation of radiating $N_2(C)$ levels for positive (upper two rows) and negative (bottom two rows) polarities of the tip. $d = 14$ mm.

electric field at the wire surface in a (1-D) wire-cylinder gap remains at the corona onset value, is widely used in the corona discharge theory and can be traced back to a classic work of Townsend of 1914 [28]. It is remarkable that in the case considered here this assumption is valid in a two-dimensional geometry.

The computed axial distribution of the electric field in the negative corona [Fig. 5(b)] is quite different. The electric field in the ionization region increases appreciably with increasing discharge voltage. Thus, the Townsend–Kaptzov assumption is not valid in this case. The width of the ionization region decreases substantially with increase in U. At high voltages,

a local minimum in E at the outer boundary of the ionization region is formed. Note that the ionization integral, evaluated along the discharge axis over the ionization region, varies with voltage between 7.7 and 9.2, i.e., not very strongly.

Fig. 6 shows the distributions of normalized densities $j(\theta)/j(0)$ and $j_{el}(\theta)/j(0)$ of the total and electron currents over the plane electrode, in negative corona discharges at the current $I = 100\ \mu$A, in two gaps, with the lengths of 5 and 14 mm. Here, θ is the angle between the axis and the line connecting the tip and the point of the plane being considered. The electron current gives a substantial contribution to the total current for both gaps. The ratio $j_{el}(0)/j(0)$ at the axis and the width of the $j_{el}(\theta)/j(0)$ distribution are larger in the smaller gap; a result that is easy to understand: fraction of the electrons that attach, during their drift from the ionization region to the plane electrode, to oxygen molecules is lower for the smaller gap, hence the contribution of electron current is higher.

The effect of shortening of the gap in the negative corona is demonstrated also in Fig. 7, where axial distributions of the normalized densities of the currents transported by the positive ions, $j_p(z)/j(z)$, the negative ions, $j_n(z)/j(z)$, and the electrons, $j_{el}(z)/j(z)$, are shown for $I = 100\,\mu$A. The current j_p dominates current transport in the ionization region, j_{el} gives the major contribution in a part of the drift zone adjacent to the ionization region, and j_n comes into play in the outer part of the drift zone. The distance l from the cathode where the values of j_n and j_{el} become comparable (the attachment length) is, for both gaps, of about 3 mm.

In long gaps, where $d/l \gg 1$, the corona current in the most part of the drift zone is transported by the negative ions. As the mobilities of the negative and positive ions are close to each other, the difference between the CVCs of negative and positive coronas for longer gaps is lower than for shorter ones, as seen in Fig. 3.

Spatial distributions of the intensity of visible radiation emitted by corona discharges differ substantially depending on the tip polarity. Fig. 8 shows the computed distributions (on a logarithmic scale) of the excitation rate R_C of radiating nitrogen states $N_2(C)$, which are the main source of visible radiation emitted by air coronas for both polarities. It was evaluated as $R_C = K_C n_{N_2} n_e$, where K_C is the excitation rate constant, which is governed by the local reduced electric field value and was found with the use of the online version of the Bolsig+ solver [16] and the cross sections [17], n_e is the electron density, and n_{N_2} is the number density of the nitrogen molecules. Also shown in Fig. 8 are the images of positive and negative coronas for various applied voltages, recorded in the experiment.

According to both the computations and the experiment, radiating regions in the positive corona have smaller sizes than those in the negative corona for comparable applied voltages and are positioned closer to the needle. These polarity effects are caused by the differences in spatial distributions of n_e and E (governing R_C values) in the high-field zone near the tip. In particular, the maximum of n_e in the ionization regions of positive coronas occurs at the needle surface, so that R_C is the highest at the surface as well. In negative coronas, n_e increases in the direction to the plane electrode, reaching the maximum at the boundary between ionization and drift regions. As a result, the maximum of R_C in this case occurs at some distance from the tip. A peculiar spatial distribution of the radiation intensity in negative coronas, seen in the bottom two rows of Fig. 8, was obtained also in [6] and is governed by the specifics of n_e and E distributions. In particular, a radial constriction of the electric field at the tip [Fig. 4(b)] results in a constriction of the radiation intensity.

V. Conclusion

The use of a stationary solver, which solves steady-state equations by means of an iterative process unrelated to time relaxation, allows one to develop a very fast and robust numerical model for evaluation of time-averaged characteristics of corona discharges. The model is implemented with the use of a detailed kinetic scheme of plasmachemical processes in ambient air taken from a preceding work [13] and involving positive and several negative ion species, and is applied to positive and negative dc corona discharges in point-plane gaps in air. A wide range of currents of both polarities and various gap lengths are investigated and the simulation results are validated by comparing the computed current–voltage characteristics and spatial distributions of the radiation intensity with the experimental data.

The calculated current–voltage characteristics are in good agreement with the measured data. This supports the choice of the set of ion mobilities that are proposed in this work with account of the possible formation of complex and cluster ions in the drift zone of corona discharges in air. Note that simulations performed with these mobility values give the current–voltage characteristics that are in good agreement with the experiment also for other geometries of corona discharges in air [21], [29]. The time-average electric field distribution in a negative corona discharge in an axially symmetric wire-cylinder gap in air, computed by means of this model, is in good agreement with the measurements [30], as shown in [29].

Computational and experimental results show that average currents I_n in negative coronas are several times higher than the currents I_p in positive coronas for the same gap length and applied voltage, the ratio I_n/I_p being smaller in longer gaps. Calculated distributions, along the discharge axis and along the plane electrode, of contributions of electrons and negative ions to the total current density in negative coronas show that the fraction of the electrons that attach to O_2 molecules during the drift of electrons, produced in the ionization region, to the plane anode, is lower for smaller gaps, thus ensuring a higher contribution of the current transported by the electrons to the total current and hence a higher I_n/I_p ratio.

The spatial distributions of the intensity of the corona discharge radiation are computed. Although only a thin region adjacent to the tip emits radiation in positive coronas, the radiating region in negative coronas is much wider and has a rather complex structure. For both polarities, specific features of the calculated distributions of radiation intensity are in a reasonable agreement with the experimental data.

One of the advantages that stationary solvers offer in simulations of steady-state discharges, when compared to

TABLE I

COMPUTATION OF SOLUTIONS FOR $U = 5.05$ AND 5.1 kV STARTING FROM THE SOLUTION FOR $U = 5$ kV. POSITIVE CORONA, GAP 5 mm. SS: STATIONARY SOLVER COMPUTATION TIME. TDS: TIME-DEPENDENT SOLVER COMPUTATION TIME

U (kV)	I (μA)	SS	TDS
5.0	3.76	–	–
5.05	4.03	39 s	58 min
5.1	4.29	50 s	5 h20 min

standard approaches that rely on time-dependent solvers, is the fact that stationary solvers are not subject to the Courant–Friedrichs–Lewy criterion or analogous limitations on the mesh element size. The removal of limitations on the mesh element is particularly important for modeling of discharges with strongly varying length scales, as is the case of corona discharges. In the modeling of this work the mesh element size varied from fractions of micrometer at the corona electrode surface to tens of micrometers far away from the corona electrode and the reduction of computation time was dramatic. An example is shown in Table I. The task was to compute the solutions for $U = 5.05$ and 5.1 kV by means of stationary and time-dependent solvers, using the previously computed solution for $U = 5$ kV as an initial approximation or the initial condition, respectively. The mesh in all the computations was the same and included 14 500 finite elements. The damping factor in all the computations and the time stepping in the time-dependent solver were set to automatic/default. The computation times shown in the table refer to a computer with a CPUs with four cores, having the clock rate of 4 GHz. Criterion for defining the computation time for the time-dependent solver was the discharge current to be within 10^{-3} of its final value, which happened within approximately 1 ms of the discharge development. One can see that the stationary solver is by several orders of magnitude faster than the time-dependent solver.

It is interesting to note that it was not possible to perform similar computations by means of the time-dependent solver for the negative corona, presumably because the glow negative corona is unstable. In this case, the time-dependent solver can be used to study the spatiotemporal evolution of the discharge, however, it is not suitable for a direct calculation of time-averaged characteristics. This illustrates another useful feature of stationary solvers: they allow decoupling of physical and numerical stability. Further examples of manifestation of this feature in gas discharge modeling can be found in [31].

ACKNOWLEDGMENT

The authors would like to thank V. S. Kuznetsov and E. A. Sosnin for the help in the experiments.

REFERENCES

[1] T. N. Tran, I. O. Golosnoy, P. L. Lewin, and G. E. Georghiou, "Numerical modelling of negative discharges in air with experimental validation," *J. Phys. D, Appl. Phys.*, vol. 44, no. 1, Dec. 2010, Art. no. 015203.

[2] P. Dordizadeh, K. Adamiak, and G. S. Peter Castle, "Numerical investigation of the formation of trichel pulses in a needle-plane geometry," *J. Phys. D, Appl. Phys.*, vol. 48, no. 41, Sep. 2015, Art. no. 415203.

[3] Y. Zheng, L. Wang, D. Wang, and S. Jia, "Numerical study of the effect of the needle tip radius on the characteristics of trichel pulses in negative corona discharges," *Phys. Plasmas*, vol. 24, no. 6, Jun. 2017, Art. no. 063515.

[4] S. Chen, K. Li, and S. Nijdam, "Transition mechanism of negative DC corona modes in atmospheric air: From trichel pulses to pulseless glow," *Plasma Sour. Sci. Technol.*, vol. 28, no. 5, May 2019, Art. no. 055017.

[5] L. Liu and M. Becerra, "An efficient model to simulate stable glow corona discharges and their transition into streamers," *J. Phys. D, Appl. Phys.*, vol. 50, no. 10, Mar. 2017, Art. no. 105204.

[6] Y. K. Stishkov, A. V. Samusenko, and I. A. Ashikhmin, "Corona discharge and electrogasdynamic flows in the air," *Physics-Uspekhi*, vol. 61, no. 12, pp. 1213–1226, Dec. 2018.

[7] M. Abdel-Salam and N. L. Allen, "Current–voltage characteristics of corona in rod–plane gaps as influenced by temperature," *IEE Proc.-Sci., Meas. Technol.*, vol. 150, no. 3, pp. 135–139, May 2003.

[8] P. Atten, K. Adamiak, B. Khaddour, and J. Fourier, "Simulation of corona discharge in configurations with sharp electrode," *J. Optoelectron. Adv. Mater.*, vol. 6, pp. 1023–1028, Sep. 2004.

[9] K. Adamiak, V. Atrazhev, and P. Atten, "Corona discharge in the hyperbolic point-plane configuration: Direct ionization criterion versus an approximate formulations," *IEEE Trans. Dielectrics Electr. Insul.*, vol. 12, no. 5, pp. 1015–1024, Oct. 2005.

[10] X. Bian, L. Wang, J. K. Macalpine, Z. Guan, J. Hui, and Y. Chen, "Positive corona inception voltages and corona currents for air at various pressures and humidities," *IEEE Trans. Dielectrics Electr. Insul.*, vol. 17, no. 1, pp. 63–70, Feb. 2010.

[11] K. Yanallah and F. Pontiga, "A semi-analytical stationary model of a point-to-plane corona discharge," *Plasma Sour. Sci. Technol.*, vol. 21, no. 4, Jul. 2012, Art. no. 045007.

[12] N. Monrolin, O. Praud, and F. Plouraboué, "Revisiting the positive DC corona discharge theory: Beyond Peek's and Townsend's law," *Phys. Plasmas*, vol. 25, no. 6, Jun. 2018, Art. no. 063503.

[13] N. G. C. Ferreira, D. F. N. Santos, P. G. C. Almeida, G. V. Naidis, and M. S. Benilov, "Simulation of pre-breakdown discharges in high-pressure air. I: The model and its application to corona inception," *J. Phys. D, Appl. Phys.*, vol. 52, no. 35, Jul. 2019, Art. no. 355206.

[14] A. Bourdon *et al.*, "Efficient models for photoionization produced by non-thermal gas discharges in air based on radiative transfer and the Helmholtz equations," *Plasma Sour. Sci. Technol.*, vol. 16, p. 656, Aug. 2007.

[15] R. S. Sigmond, "The residual streamer channel: Return strokes and secondary streamers," *J. Appl. Phys.*, vol. 56, no. 5, pp. 1355–1370, Sep. 1984.

[16] G. J. M. Hagelaar and L. C. Pitchford, "Solving the Boltzmann equation to obtain electron transport coefficients and rate coefficients for fluid models," *Plasma Sour. Sci. Technol.*, vol. 14, no. 4, pp. 722–733, Nov. 2005.

[17] *Phelps Database*. Accessed: Jan. 29, 2019. [Online]. Available: https://www.lxcat.net

[18] A. V. Filippov *et al.*, "Ionic composition of a humid air plasma under ionizing radiation," *J. Exp. Theor. Phys.*, vol. 125, no. 2, pp. 246–267, Aug. 2017.

[19] L. A. Viehland and E. A. Mason, "Transport properties of gaseous ions over a wide energy range, IV," *At. Data Nucl. Data Tables*, vol. 60, pp. 37–95, May 1995.

[20] H. Böhringer, D. W. Fahey, W. Lindinger, F. Howorka, F. C. Fehsenfeld, and D. L. Albritton, "Mobilities of several mass-identified positive and negative ions in air," *Int. J. Mass Spectrometry Ion Processes*, vol. 81, pp. 45–65, Dec. 1987.

[21] P. G. C. Almeida, R. M. S. Almeida, N. G. C. Ferreira, G. V. Naidis, and M. S. Benilov, "Simple computation of ignition voltage of self-sustaining gas discharges," *Plasma Sources Sci. Technol.*, to be published, doi: 10.1088/1361-6595/abbf91.

[22] T. R. Foord, "Some experiments on positive point-to-plane corona and spark breakdown of compressed gases," *Proc. IEE II, Power Eng.*, vol. 100, no. 78, pp. 585–590, Dec. 1953.

[23] A. Takahashi and K. Nishijima, "Laser-induced breakdown characteristics of nonuniform DC corona discharge fields," *IEEE Trans. Dielectrics Electr. Insul.*, vol. 1, no. 4, pp. 590–596, Aug. 1994.

[24] A. F. Gutsol and W. R. Pyle, "Negative corona 'tufts,"' *Plasma Sources Sci. Technol.*, vol. 23, no. 5, Sep. 2014, Art. no. 054015.

[25] G. F. L. Ferreira, O. N. Oliveira, and J. A. Giacometti, "Point-to-plane corona: Current-voltage characteristics for positive and negative polarity with evidence of an electronic component," *J. Appl. Phys.*, vol. 59, no. 9, pp. 3045–3049, 1986.

[26] S. Chen, R. G. W. van den Berg, and S. Nijdam, "The effect of DC voltage polarity on ionic wind in ambient air for cooling purposes," *Plasma Sources Sci. Technol.*, vol. 27, no. 5, May 2018, Art. no. 055021.
[27] P. Y. Raizer, *Gas Discharge Physics*. Berlin, Germany: Springer, 1991.
[28] J. S. Townsend, "XI. The potentials required to maintain currents between coaxial cylinders," *London, Edinburgh, Dublin Phil. Mag. J. Sci.*, vol. 28, no. 163, pp. 83–90, Jul. 1914.
[29] N. G. C. Ferreira, P. G. C. Almeida, M. S. Benilov, and G. V. Naidis, "Comment on 'Electric field measurements under DC corona discharges in ambient air by electric field induced second harmonic generation' [Appl. Phys. Lett. 115, 244101 (2019)]," *Appl. Phys. Lett.*, vol. 117, no. 2, 2020, Art. no. 026101.
[30] Y. Cui, C. Zhuang, and R. Zeng, "Electric field measurements under c corona discharges in ambient air by electric field induced second harmonic generation," *Appl. Phys. Lett.*, vol. 115, no. 24, 2019, Art. no. 244101.
[31] P. G. C. Almeida, M. S. Benilov, M. D. Cunha, and J. G. L. Gomes, "Computing different modes on cathodes of DC glow and high-pressure arc discharges: Time-dependent versus stationary solvers," *Plasma Processes Polym.*, vol. 14, nos. 4–5, Apr. 2017, Art. no. 1600122.

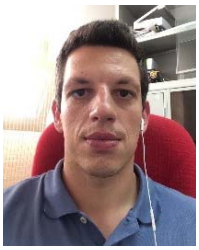

Nuno G. C. Ferreira was born in Madeira, Portugal, in 1982. He received the B.Sc. degree in telecommunications and networks engineering from the University of Madeira, Madeira, in 2005, and the Ph.D. degree in electrical engineering from the University of Aveiro, Aveiro, Portugal, in 2019.

Since 2017, he has been with the Institute for Plasmas and Nuclear Fusion, Instituto Superior Técnico, Universidade de Lisboa, Lisbon, Portugal. He is currently an invited Assistant Professor with the Department of Exact Sciences and Engineering, University of Madeira, where he has been working since 2008. His current research interests include numerical simulation of corona and streamer discharges.

Pedro G. C. Almeida received the Ph.D. degree in physics from the University of Madeira, Madeira, Portugal, in 2011. His thesis focused on theory, modeling and experiments on different modes of current transfer to cathodes of glow and arc discharges.

Since 2015, he has been with the Institute for Plasmas and Nuclear Fusion, Instituto Superior Técnico, Universidade de Lisboa, Lisbon, Portugal. He is currently an Assistant Professor with the Department of Physics, University of Madeira, where he has been working since 2001. His current research interests include theory and modeling of glows, coronas and streamers, self-organization phenomena in gas discharges, and modes of current transfer to cathodes of gas discharges.

Mikhail S. Benilov received the diploma degree (Hons.) and the C.Sc. (Ph.D.) degree in physics from the Moscow Institute for Physics and Technology, Moscow, Russia, in 1974 and 1978, respectively, and the Doctor of Physical and Mathematical Sciences degree from the Institute for High Temperatures, USSR Academy of Sciences, Moscow, in 1990. His thesis focuses on theory of electrostatic probes and electrodes in high-pressure flowing plasmas.

He had been with the Institute for High Temperatures, USSR Academy of Sciences, Moscow, where he led a group working in plasma and nonlinear physics, numerical modeling, and fluid dynamics, after completing postgraduate courses with the Moscow Institute for Physics and Technology and the Institute for Mechanics of Lomonosov Moscow State University, Moscow, in 1977. Since 1993, he has been a Professor with the Departamento de Física, Universidade da Madeira, Madeira, Portugal. Since 2015, he also leads a High-Pressure Plasmas Group, Instituto de Plasmas e Fusão Nuclear, Instituto Superior Técnico, Universidade de Lisboa. His current research interests include plasma physics, in particular, plasma-electrode interaction, kinetic theory of phase transitions, and numerical modeling.

Dr. Benilov received the Alexander von Humboldt Research Fellowship in 1990 and stayed for 2 years with the Ruhr-Universität Bochum, Germany, working on the theory and simulation of near-electrode phenomena.

Victor A. Panarin received the Ph.D. degree in optics from Tomsk State University, Siberia, Russia, in 2019. He is currently a Researcher with the Optical Radiation Laboratory, Institute of High-Current Electronics SB RAS, Tomsk, Russia.

He is a coauthor of 125 publications, 10 inventions, 2 reviews, and 1 monographs. His research interests lie in the physics of gas discharges, spontaneous sources of UV and VUV radiation (excilamps) and their application, and in pulsed dense gas lasers.

Victor S. Skakun received the Ph.D. degree in laser physics from Tomsk State University, Siberia, Russia, in 1988.

He is currently a Senior Researcher with the Optical Radiation Laboratory, Institute of High Current Electronics SB RAS, Tomsk, Russia. He has coauthored more than 279 publications and 39 inventions. His research interests are in physics of gas discharges and spontaneous UV and VUV sources (excilamps) and their application.

Victor F. Tarasenko received the Ph.D. and D.Sc. degrees in laser physics from Tomsk State University, Siberia, Russia, in 1976 and 1988, respectively.

He was a Professor in 1994. He is currently a Chief Researcher with the Optical Radiation Laboratory, Institute of High Current Electronics SB RAS, Tomsk, Russia, and a Professor with Tomsk State University, Tomsk, and Tomsk Polytechnic University, Tomsk. He has coauthored more than 900 publications, 70 inventions, 23 reviews, 11 monographs, and 3 textbooks for students. His research interests are in physics of gas discharges and generation of runaway electrons, spontaneous UV and VUV sources (excilamps) and their application, dense-gas pulsed lasers.

Dr. Tarasenko is a member of the Editor board of Journals *Laser and Particle Beams*, *Atmospheric and Oceanic Optics*, *Quantum Electronics*, and *High Voltage*.

George V. Naidis received the degree from Moscow State University, Moscow, Russia, in 1969, and the Ph.D. and D.Sc. degrees in plasma physics and chemistry from the Joint Institute for High Temperatures of the Russian Academy of Sciences, Moscow, in 1977 and 1993, respectively.

Since 1971, he has been with the Joint Institute for High Temperatures, Moscow, where he is currently a Principal Researcher. He has coauthored more than 300 scientific publications. His research interests include physical and chemical kinetics of low-temperature plasma, physics of gas discharges and gas dynamics.